Nanoscale

PAPER

View Article Online
View Journal | View Issue

Cite this: *Nanoscale*, 2014, **6**, 7033

A flux induced crystal phase transition in the vapor–liquid–solid growth of indium-tin oxide nanowires†

Gang Meng,[a] Takeshi Yanagida,*[a] Hideto Yoshida,[a] Kazuki Nagashima,[a] Masaki Kanai,[a] Fuwei Zhuge,[a] Yong He,[a] Annop Klamchuen,[a] Sakon Rahong,[a] Xiaodong Fang,[b] Seiji Takeda[a] and Tomoji Kawai[a]

Received 24th February 2014
Accepted 3rd April 2014

DOI: 10.1039/c4nr01016g

www.rsc.org/nanoscale

Single crystalline metal oxide nanowires formed *via* a vapor–liquid–solid (VLS) route provide a platform not only for studying fundamental nanoscale properties but also for exploring novel device applications. Although the crystal phase variation of metal oxides, which exhibits a variety of physical properties, is an interesting feature compared with conventional semiconductors, it has been difficult to control the crystal phase of metal oxides during the VLS nanowire growth. Here we show that a material flux critically determines the crystal phase of indium-tin oxide nanowires grown *via* the VLS route, although thermodynamical parameters, such as temperature and pressure, were previously believed to determine the crystal phase. The crystal phases of indium-tin oxide nanowires varied from the rutile structures (SnO_2), the metastable fluorite structures ($In_xSn_yO_{3.5}$) and the bixbyite structures (Sn-doped In_2O_3) when only the material flux was varied within an order of magnitude. This trend can be interpreted in terms of the material flux dependence of crystal phases (rutile SnO_2 and bixbyite In_2O_3) on the critical nucleation at the liquid–solid (LS) interface. Thus, precisely controlling the material flux, which has been underestimated for VLS nanowire growths, allows us to design the crystal phase and properties in the VLS nanowire growth of multicomponent metal oxides.

1 Introduction

Single crystalline nanowires composed of metal oxides offer an interesting research platform not only for investigating fundamental nanoscale properties of metal oxides but also for exploring novel engineering applications by utilizing the unique and robust properties in air and/or water.[1–4] Among various nanowire growth methods, a vapor–liquid–solid (VLS) method has proven great potential to synthesize well-defined single crystalline nanowires. In the VLS nanowire growth, the size and spatial position of nanowires are readily controllable by adjusting the size and spatial position of the metal catalyst.[5–7] In addition, the heterostructures along axial or radial directions can be sequentially designed by using the VLS process.[8–11] These unique and fascinating features of the VLS method are not attainable by other nanowire growth methods.[12]

Metal oxides exhibit various fascinating physical properties including ferroelectric, ferromagnetism, transparent conducting, superconducting and others, which are not attainable by conventional semiconductors.[13–16] The crystal phase variation of metal oxides plays an important role on a variety of such fascinating physical properties. The crystal phase variation for oxide thin films has been controlled by varying the surrounding thermodynamical conditions including temperature and pressure.[17,18] The crystal phase variation should also be appropriately controlled for the VLS nanowire growth of metal oxides to attain the desired physical properties. Unfortunately, the wide range control of thermodynamical conditions, which has been applied to oxide thin film formations, is not applicable to the VLS nanowire growth due to the narrow window of surrounding conditions required for the VLS nanowire growth.[19] In this study, we propose a strategy to control the crystal phase of metal oxides during VLS nanowire growth. We demonstrate that a material flux critically determines the crystal phase stability during the VLS nanowire growth of indium-tin oxides. Although thermodynamical conditions were previously believed to determine the crystal phase of VLS nanowires, we found that the slight flux difference induces the completely different crystal phases of indium-tin oxide nanowires.

[a]*Institute of Scientific and Industrial Research, Osaka University, 8-1 Mihogaoka, Osaka, Ibaraki, Japan. E-mail: yanagi32@sanken.osaka-u.ac.jp; Fax: +81-06-6879-4295; Tel: +81-06-6879-4294*

[b]*Anhui Institute of Optics and Fine Mechanics, Chinese Academy of Sciences, Hefei 230031, China*

† Electronic supplementary information (ESI) available: STEM mapping of In and Sn in an ISO nanowire (Fig. S1) and homogeneity of a fluorite ISO phase at the full length of a nanowire (Fig. S2). See DOI: 10.1039/c4nr01016g

2 Experimental section

Indium-tin oxide nanowires were fabricated by the vapor–liquid–solid (VLS) method using pulsed laser deposition (PLD).[19–25] Prior to the nanowire growth, the chamber was evacuated to a base pressure of 5×10^{-6} Pa. Then the oxygen and Ar mixed gas (the molar ratio of $O_2 : Ar = 1 : 10^6$) was introduced into the chamber. The total pressure of the chamber was maintained to be 10 Pa. After heating the MgO(100) substrate (with 0.7 nm Au layer) up to the growth temperature of 750 °C, the SnO_2 and In_2O_3 mixed target (the molar ratio of Sn : In = 80 : 20) was ablated using an ArF excimer laser (λ = 193 nm, repetition rate = 10 Hz). The supplied metal fluxes were controlled by tuning the laser power from 25 mJ to 60 mJ. We analyzed the supplied metal fluxes by measuring the volume of thin films deposited under room-temperature, where the evaporation events on the substrate were negligible. The volume of thin films was measured using a surface profiler (Alpha-Step IQ), and then the metal fluxes were estimated by the material density.[19] The compositions of supplied fluxes were measured using an electron probe micro-analyzer (EPMA, JEOL, JXA-8800R). Further details of the nanowire growth process can be seen elsewhere.[24,25] The morphologies of nanowires were observed using the field emission scanning electron microscope (FESEM, JEOL, JSM-7001F). The crystallinity, phase and element concentration of nanowires were examined using the high-resolution transmission electron microscope (HRTEM, JEOL JEM-ARM200F), equipped with energy dispersive spectroscopy (EDS) and selected area electron diffraction (SAED). The transport properties of nanowires were measured with the semiconductor parameter analyzer (Keithley 4200SCS).

3 Results and discussion

Fig. 1 shows the effect of material flux on the SEM, TEM, SAED and EDS data of fabricated indium-tin oxide nanowires. The material flux was varied from 2×10^{17} to 16×10^{17} (metal atoms cm^{-2} s^{-1}) within an order of magnitude, and the other conditions were set to be constant. These nanowires were grown by using the tin-rich target of Sn : In in the molar ratio of 80 : 20. When the total material flux was relatively low – 2×10^{17} cm^{-2} s^{-1}, the fabricated nanowires only showed the rutile crystal phase (space group: $P4_2/mnm$) of SnO_2 without the significant indium component, as shown in EDS data of Fig. 1a. When we increased the material flux to 6×10^{17} cm^{-2} s^{-1}, the fabricated nanowires exhibited the metastable fluorite crystal phase (space group: $Fm\bar{3}m$) of $In_xSn_yO_{3.5}$ (so-called ISO phase[26]). The fluorite phase was confirmed by electron diffraction analysis taken along [001] and [011] directions, as shown in the upper and lower SAED data in Fig. 1b. Note that these nanowires are entirely composed of the metastable ISO crystal phase, which is in sharp contrast to previous reports that showed the partial ISO crystal phase within nanowires.[24,26] The detailed microstructural analysis of ISO nanowires can be seen

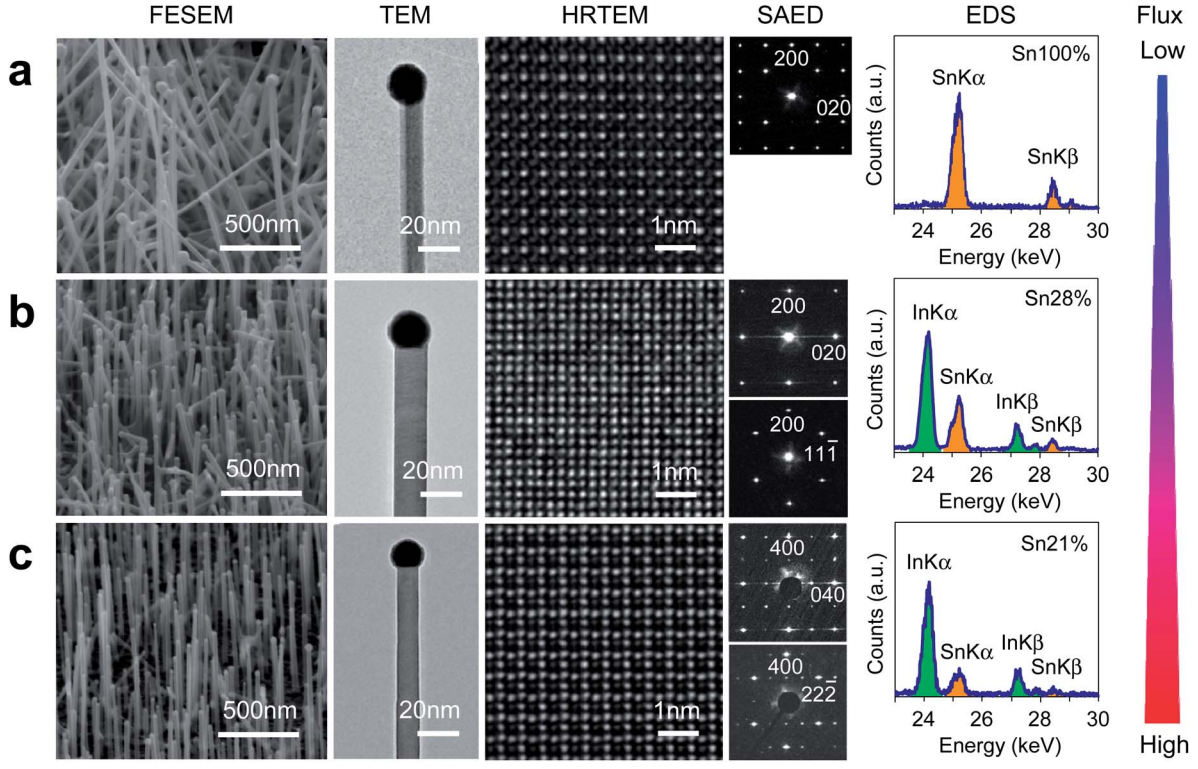

Fig. 1 SEM, TEM, HRTEM, SAED and EDS data of indium-tin oxide nanowires when varying the supplied Sn/In fluxes: (a) data for the flux of 2×10^{17} cm^{-2} s^{-1}. (b) Data for the flux of 6×10^{17} cm^{-2} s^{-1}, the upper ED data were taken along [001] and the lower data were taken along the [011] orientation. (c) Data for the flux of 16×10^{17} cm^{-2} s^{-1}, the upper ED data were taken along the [001] and the lower one was taken along the [011] orientation.

in ESI – Fig. S1.† When the material flux was further increased to 16 × 10^{17} cm^{-2} s^{-1}, the fabricated nanowires were of a bixbyite crystal phase (space group: *Ia*3) of the conventional Sn-doped In_2O_3 (ITO), as shown in Fig. 1c. Thus, interestingly the material flux strongly influences the crystal phase of fabricated nanowires even when using the constant of other experimental configurations for VLS nanowire growths. Although the tin concentration of the target source was constant for all VLS nanowire growths, the tin concentration incorporated into nanowires was significantly different when varying only the material fluxes, as seen in the EDS data of Fig. 1. Fig. 2 shows the effect of material flux on the series of tin concentration data incorporated into nanowires, which were measured by TEM-EDS. We define the tin concentration (%) as (Sn/(Sn + In)) × 100. Other growth conditions were the same as those for the growth experiments of Fig. 1. Below 4 × 10^{17} cm^{-2} s^{-1} of the material flux, the tin concentration was almost 100% with the rutile crystal phase of SnO_2. In the middle material flux range (6 × 10^{17}–14 × 10^{17} cm^{-2} s^{-1}), the tin concentration was around 30% with the fluorite crystal phase of metastable ISO. For the higher material flux range – 16 × 10^{17} cm^{-2} s^{-1}, the tin concentration decreased to around 20% with the bixbyite crystal phase of ITO. It is noted that these structural and composition variations occur within an order of magnitude of the material flux. These experimental data highlight that the material flux, which was previously believed to affect solely the growth rate,[19,27] determines the crystal phase of nanowires formed *via* the VLS route.

Here, we discuss the inherent mechanisms of how the material flux affects the crystal phase of indium-tin oxide nanowires during the VLS growth. Firstly, we examine the composition difference between the target source and the material species supplied onto the substrate when the material flux was varied. This is because the material composition supplied from the target might be altered when the laser power of ablation is varied to change the material flux. We measured the material composition supplied onto the substrate by performing the composition measurements of films deposited under room temperature, where the evaporation events are negligible.[19,28] As shown in the inset of Fig. 2, the measured tin concentration was nearly consistent with the nominal target composition (80%) independent of the material flux variation. Thus, we can exclude the scenario based on the composition variation of the supplied species on the crystal phase variation in the VLS nanowires of indium-tin oxides.

Next, we consider the nucleation probability of indium and tin at the liquid–solid (LS) interface to explain the crystal phase variations of nanowires. This is because, in principle, the crystal nucleation at the LS interface determines the crystal phase of VLS grown nanowires.[29] When both indium and tin elements exist within the metal catalysts,[30] the crystals formed at the LS interface can be various crystal phases comprised of indium, tin and oxygen. If the different crystal phases have different critical material fluxes for nucleation,[31] the critical flux dependence of different crystal phases might explain the present experimental results of Fig. 1 and 2.

Although the complete understanding requires the knowledge as to the thermodynamics and kinetics of nucleation of all components of Sn–In–O–Au (including the phase diagram), such information of multicomponent systems is unfortunately not available. As an alternative experimental approach to obtain an insight into the nucleation events of tin and indium elements at the LS interface, we measured the critical material flux for the nucleation at the LS interface of the parent compounds – In_2O_3 and/or SnO_2. We measured the growth rate of nanowires when varying the material fluxes, as shown in

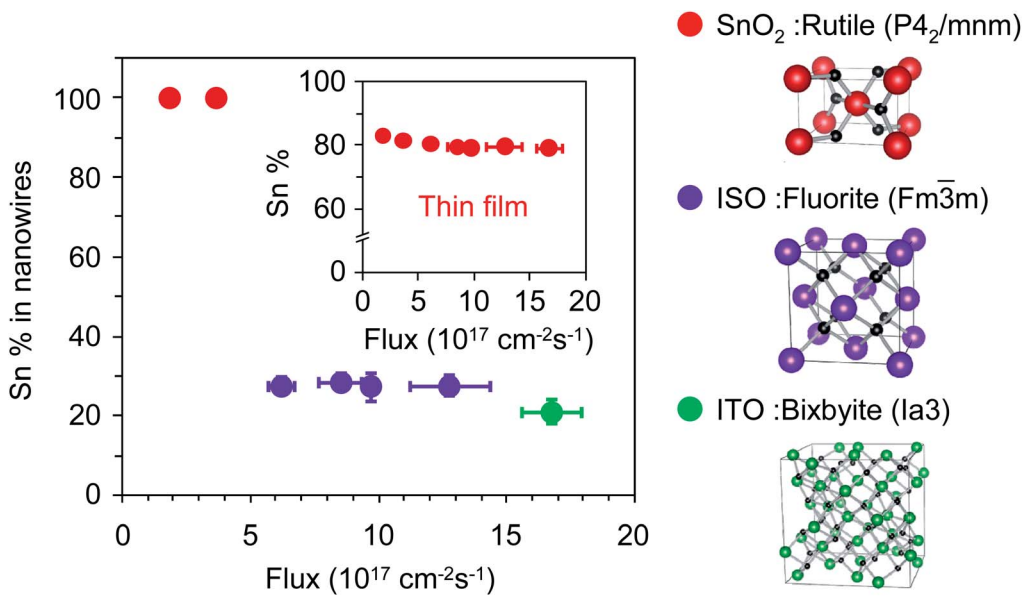

Fig. 2 The incorporated tin concentration data of nanowires, measured by EDS, when increasing the supplied Sn/In flux. The detailed crystal structural information of obtained single crystalline nanowires was shown on the right side. The inset figure shows the tin concentration data of thin films deposited at room temperature which were measured by EPMA.

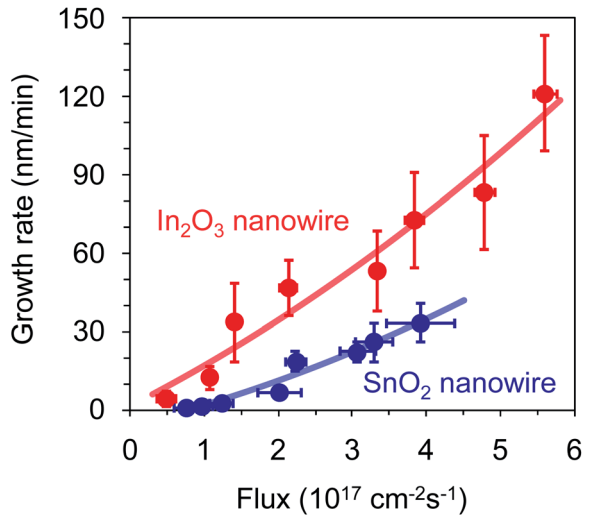

Fig. 3 Critical fluxes for nucleation of the parent compounds (bixbyite In_2O_3 and rutile SnO_2 nanowires) when varying the material fluxes.

Fig. 3. The *x*-axis of Fig. 3 is the metal flux of each pure component, whereas the *x*-axis of Fig. 2 is the total metal flux of the mixed supply. The same experimental configurations (temperature, pressure and others) in Fig. 1 and 2 were employed for these nanowire growth experiments. As can be seen, the critical flux for the nucleation of In_2O_3 nanowires is lower than that for SnO_2 nanowires. This difference is due to their different energy barrier heights for the nucleation at the LS interface, as discussed in previous studies.[24,31] This experimental trend of Fig. 3 can be utilized to semi-quantitatively explain the crystal phase variation of Fig. 1 and 2 in the VLS growth in terms of the critical material flux values, as given below.

For the total mixed flux range below 4×10^{17} cm^{-2} s^{-1} (*i.e.*, 0.8×10^{17} cm^{-2} s^{-1} for indium and 3.2×10^{17} cm^{-2} s^{-1} for tin), only the SnO_2 crystal phase can nucleate at the LS interface. This is because the material flux for tin only exceeds the critical flux for SnO_2, whereas the material flux for indium is still below the critical flux for the In_2O_3 crystal phase. In this range, the supplied indium species must evaporate to the vapor phase during the VLS growth. In addition, indium species within Au catalysts cannot be incorporated into rutile SnO_2 nanowires due to low solubility.[24] For the total mixed flux range around 4–6 $\times 10^{17}$ cm^{-2} s^{-1}, the material flux for indium can exceed the critical flux for In_2O_3 when considering the use of the present indium 20% target. *i.e.*, the indium flux is 0.8–1.2 $\times 10^{17}$ cm^{-2} s^{-1}, which is interestingly in good agreement with the critical flux for In_2O_3 nanowires in

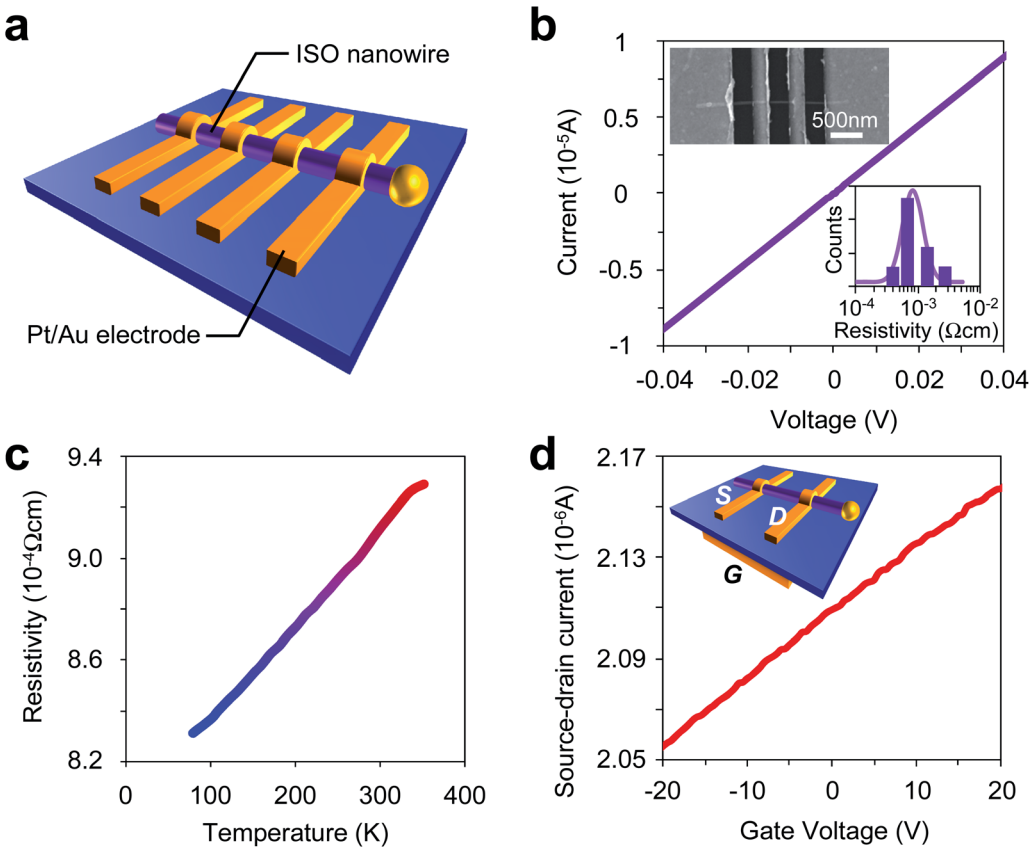

Fig. 4 Transport properties of single crystalline ISO nanowires. (a) A schematic image of the transport measurement system for ISO nanowires. (b) A typical *I*–*V* curve of ISO nanowires using the four-probe measurement system. The inset figure shows the resistivity distribution data, and the inset image shows the SEM data of the fabricated measurement system. (c) Typical temperature dependence data of resistivity (ρ–*T*) of ISO nanowires and (d) Field effect measurement data. The inset shows the configuration of a field effect transistor (FET).

Fig. 3. Thus, once the nucleation for In_2O_3 at the LS interface emerges, indium-rich fluorite ISO nanowires were formed *via* the VLS route. In addition, our experimental results demonstrate that the emerged nucleation of In_2O_3 fully suppressed the growth of the SnO_2 rutile phase at the LS interface. The preferential nucleation of In_2O_3 at the LS interface can be interpreted in terms of the thermodynamical stability of each compound (*e.g.* the melting points of In_2O_3 – 1910 °C and SnO_2 – 1630 °C).[24] Considering the thermodynamical stability, tin species within catalysts can be easily incorporated into the In_2O_3 – based compounds rather than forming SnO_2 crystal structures at the LS interface, although the direct experimental evidence as to the physical events at the LS interface should be examined by *in situ* measurement techniques.[32,33] Further increasing the mixed material flux above 15×10^{17} cm^{-2} s^{-1} resulted in the change from ISO to the ITO crystal phase, which can be qualitatively explained in terms of the increased indium composition within nanowires *via* the increased growth rate of In_2O_3 compounds at the LS interface as seen in Fig. 3. Although the exact nucleation mechanisms of multicomponent systems at the LS interface are still open questions, the present simple model based on the presence of different critical material fluxes for various crystal phases gives a rigorous qualitative explanation for the material flux dependence on the crystal phase of indium-tin oxide VLS nanowires. This approach should be applicable to various VLS growths of multicomponent metal oxides to experimentally design the crystal phase.

Finally, we examine the transport properties of newly fabricated metastable ISO single crystalline nanowires. This is because the ISO nanowire fabricated in this study is the first demonstration that the metastable crystal phase of indium-tin oxides can be extracted as an entire single crystalline entity,[34,35] as seen in the ESI – Fig. S2.† In previous works, ISO phases have been found as the secondary phase.[24,26] Therefore, the physical properties of ISO single phases have never been measured to date. We measured the transport properties of fabricated ISO single crystalline nanowires by utilizing the measurement system, which has been reported elsewhere.[24] As shown in Fig. 4b, we found that the ISO nanowires are conductive (resistivity range of 10^{-4} Ω cm) with metallic behavior, proved by the resistivity–temperature (ρ–T) measurement shown in Fig. 4c. The FET measurements (the back gate of 100 nm thick SiO_2) demonstrate the n-type behavior, as shown in Fig. 4d. In fact, these trends are not consistent with the predictions of ISO crystal phase properties by a first principle calculation, where they predicted the emergence of a semiconductor with the narrow band gap for the ISO phase.[36] One possible reason for this is the composition difference between the present ISO and that assumed in the calculation. Thus, the present material flux control method offers a strategy to explore new crystal phases and their properties of multicomponent metal oxide nanowires *via* the VLS route.

4 Conclusion

In summary, we demonstrated that the material flux critically determines the crystal phase of VLS nanowires composed of indium-tin oxides although surrounding thermodynamical parameters, including temperature and pressure, were previously believed to determine the crystal phase. The crystal phase of indium-tin oxide nanowires varied from the rutile structure (SnO_2), the fluorite structure (ISO) and the bixbyite structure (ITO) when only the material flux was varied within an order of magnitude. The flux induced crystal phase variation can be interpreted in terms of the material flux dependence of crystal phases (rutile SnO_2 and bixbyite In_2O_3) on the crystal nucleation at the LS interface. The present experimental results highlight that precisely controlling the material flux, which has been underestimated, is a key issue to experimentally design the crystal phase of multicomponent metal oxide nanowires *via* the VLS route.

Acknowledgements

This study was supported by NEXT. T. K. was supported by the FIRST program. A part of this work was supported by the "Low-Carbon Research Network (Handai satellite)" of Ministry of Education, Culture, Sports, Science and Technology (MEXT), Japan.

Notes and references

1 M. Law, L. E. Greene, J. C. Johnson, R. Saykally and P. D. Yang, *Nat. Mater.*, 2005, **4**, 455.
2 I. S. Cho, C. H. Lee, Y. Z. Feng, M. Logar, P. M. Rao, L. L. Cai, D. R. Kim, R. Sinclair and X. L. Zheng, *Nat. Commun.*, 2013, **4**, 1723.
3 X. Y. Yang, A. Wolcott, G. M. Wang, A. Sobo, R. C. Fitzmorris, F. Qian, J. Z. Zhang and Y. Li, *Nano Lett.*, 2009, **9**, 2331.
4 Z. L. Wang, *Adv. Mater.*, 2003, **15**, 432.
5 R. X. Yan, D. Gargas and P. D. Yang, *Nat. Photonics*, 2009, **3**, 569.
6 A. Klamchuen, T. Yanagida, M. Kanai, K. Nagashima, K. Oka, S. Rahong, M. Gang, M. Horprathum, M. Suzuki, Y. Hidaka, S. Kai and T. Kawai, *Appl. Phys. Lett.*, 2011, **99**, 193105.
7 M. T. Borgstrom, G. Immink, B. Ketelaars, R. Algra and E. P. A. M. Bakkers, *Nat. Nanotechnol.*, 2007, **2**, 541.
8 Y. Y. Wu, R. Fan and P. D. Yang, *Nano Lett.*, 2002, **2**, 83.
9 J. G. Lu, P. Chang and Z. Fan, *Mater. Sci. Eng., R*, 2006, **52**, 49.
10 O. Hayden, R. Agarwal and W. Lu, *Nano Today*, 2008, **3**, 12.
11 C. Y. Wen, M. C. Reuter, J. Bruley, J. Tersoff, S. Kodambaka, E. A. Stach and F. M. Ross, *Science*, 2009, **326**, 1247.
12 H. J. Fan, P. Werner and M. Zacharias, *Small*, 2006, **2**, 700.
13 E. Dagotto, *Science*, 2005, **309**, 257.
14 K. Nomura, H. Ohta, K. Ueda, T. Kamiya, M. Hirano and H. Hosono, *Science*, 2003, **300**, 1269.
15 M. Bibes, J. E. Villegas and A. Barthelemy, *Adv. Phys.*, 2011, **60**, 5.
16 L. Li, P. S. Lee, C. Y. Yan, T. Y. Zhai, X. S. Fang, M. Y. Liao, Y. Koide, Y. Bando and D. Golberg, *Adv. Mater.*, 2010, **22**, 5145.
17 J. S. Corneille, J. W. He and D. W. Goodman, *Surf. Sci.*, 1995, **338**, 211.

18 T. Yanagida, T. Kanki, B. Vilquin, H. Tanaka and T. Kawai, *Phys. Rev. B: Condens. Matter Mater. Phys.*, 2004, **70**, 184437.
19 F. Zhuge, T. Yanagida, K. Nagashima, H. Yoshida, M. Kanai, B. Xu, A. Klamchuen, G. Meng, Y. He, S. Rahong, X. M. Li, M. Suzuki, S. Kai, S. Takeda and T. Kawai, *J. Phys. Chem. C*, 2012, **116**, 24367.
20 K. Nagashima, T. Yanagida, K. Oka, H. Tanaka and T. Kawai, *Appl. Phys. Lett.*, 2008, **93**, 153103.
21 A. Klamchuen, T. Yanagida, K. Nagashima, S. Seki, K. Oka, M. Taniguchi and T. Kawai, *Appl. Phys. Lett.*, 2009, **95**, 053105.
22 K. Nagashima, T. Yanagida, K. Oka, M. Taniguchi, T. Kawai, J. S. Kim and B. H. Park, *Nano Lett.*, 2010, **10**, 1359.
23 K. Oka, T. Yanagida, K. Nagashima, M. Kanai, T. Kawai, J. S. Kim and B. H. Park, *J. Am. Chem. Soc.*, 2011, **133**, 12482.
24 G. Meng, T. Yanagida, K. Nagashima, H. Yoshida, M. Kanai, A. Klamchuen, F. W. Zhuge, Y. He, S. Rahong, X. D. Fang, S. Takeda and T. Kawai, *J. Am. Chem. Soc.*, 2013, **135**, 7033.
25 K. Nagashima, T. Yanagida, K. Oka, M. Kanai, A. Klamchuen, S. Rahong, G. Meng, M. Horprathum, B. Xu, F. Zhuge, Y. He, B. H. Park and T. Kawai, *Nano Lett.*, 2012, **12**, 5684.
26 J. Gao, O. I. Lebedev, S. Turner, Y. F. Li, Y. H. Lu, Y. P. Feng, P. Boullay, W. Prellier, G. Tendeloo and T. Wu, *Nano Lett.*, 2012, **12**, 275.
27 A. Marcu, T. Yanagida, K. Nagashima, H. Tanaka and T. Kawai, *J. Appl. Phys.*, 2007, **102**, 016102.
28 A. Klamchuen, T. Yanagida, M. Kanai, K. Nagashima, K. Oka, T. Kawai, M. Suzuki, Y. Hidaka and S. Kai, *Appl. Phys. Lett.*, 2010, **97**, 073114.
29 B. A. Wacaser, K. A. Dick, J. Johansson, M. T. Borgstrom, K. Deppert and L. Samuelson, *Adv. Mater.*, 2009, **21**, 153.
30 P. Nguyen, S. Vaddiraju and M. Meyyappan, *J. Electron. Mater.*, 2006, **35**, 200.
31 M. Suzuki, Y. Hidaka, T. Yanagida, A. Klamchuen, M. Kanai, T. Kawai and S. Kai, *Phys. Rev. E: Stat., Nonlinear, Soft Matter Phys.*, 2011, **83**, 061606.
32 E. Sutter and P. Sutter, *Nano Lett.*, 2008, **8**, 411.
33 S. H. Oh, M. F. Chisholm, Y. Kauffmann, W. D. Kaplan, W. D. Luo, M. Ruhle and C. Scheu, *Science*, 2010, **330**, 489.
34 S. I. Castaneda, F. Rueda, R. Diaz, J. M. Ripalda and I. Montero, *J. Appl. Phys.*, 1998, **83**, 1995.
35 P. Thilakan and J. Kumar, *Phys. Status Solidi A*, 1997, **160**, 97.
36 S. Z. Karazhanov, P. Ravindran and U. Grossner, *Thin Solid Films*, 2011, **519**, 6561.